Amide I Modes of α-Helical Polypeptide in Liquid Water: Conformational Fluctuation, Phase Correlation, and Linear and Nonlinear Vibrational Spectra

Sihyun Ham,[†] Seungsoo Hahn,[‡] Chewook Lee,[‡] Tae-Kyung Kim,[‡] Kyungwon Kwak,[‡] and Minhaeng Cho*[,‡]

Department of Chemistry, Sookmyung Women's University, Seoul 140-742, Korea, and Department of Chemistry and Center for Multidimensional Spectroscopy, Division of Chemistry and Molecular Engineering, Korea University, Seoul 136-701, Korea

Received: March 24, 2004; In Final Form: April 14, 2004

Chain length and site dependencies of amide I local mode frequencies of α-helical polyalanines are theoretically studied by carrying out semiempirical quantum chemistry calculations. A theoretical model that can be used to quantitatively predict both the local amide I mode frequencies and coupling constants between two different local amide I modes is developed. Using this theoretical model and performing molecular dynamics simulation of an α-helical polyalanine in liquid water, we investigate conformational fluctuation and hydrogen-bonding dynamics by monitoring amide I frequency fluctuations. The instantaneous normal-mode analysis method is used to obtain densities of states of the one- and two-exciton bands and to quantitatively investigate the extent of delocalization of the instantaneous amide I normal modes. Also, by introducing a novel concept of the so-called weighted phase-correlation factor, the symmetric natures of the delocalized amide I normal modes are elucidated, and it is also shown that there is no unique way to classify any given amide I normal mode of the α-helical polyalanine in liquid water to be either *A*-mode-like or E_1-mode-like. From the ensemble-averaged dipole strength spectrum and density of one-exciton states, the amide I infrared absorption spectrum is numerically calculated and its asymmetric line shape is theoretically described. Considering both transitions from the ground state to one-exciton states and those from one-exciton states to two-exciton states, we calculate the two-dimensional IR pump−probe spectra and directly compare them with recent experimental results. A brief discussion on the cross-peaks previously observed in the two-dimensional difference spectrum is presented.

I. Introduction

To establish the relationship between the secondary structure of polypeptide and amide I absorption spectrum, a number of theoretical models were presented and found to be useful.[1−14] For example, there exist several empirical rules such as (i) the amide I infrared (IR) band of an α-helix peaks at 1650 cm^{-1} and (ii) that of a β-sheet polypeptide exhibits a major peak at lower frequency region around 1630 cm^{-1}. A bit more quantitative method of predicting the hydrogen-bonding effect on the amide I mode frequency red-shift, $\delta\tilde{\nu}_I$, is to use the following empirical formula, $\delta\tilde{\nu}_I = -\alpha_{Hyd}\{2.6 - r(O\cdots H)\}$, where $r(O\cdots H)$ denotes the hydrogen-bond distance in Å and the proportionality constant α_{Hyd} was assumed to be 30 cm^{-1}/Å.[15,16] However, the authors already showed that this simple formula is not quantitatively reliable in predicting solvatochromic amide I mode frequency shift of the aqueous NMA solution.[17,18] In the case of intramolecular hydrogen-bonding effect on the amide I mode frequency shift, Brauner et al.'s empirical correction method could be of use, though it is not accurate enough to take into account 3D structure-dependency of amide I local mode frequency shift.[19]

Due to the difficulties of determining precise distributions of amide I vibrational frequencies, corresponding eigenvectors, and dipole strengths, it was only possible to qualitatively determine the existence of a given secondary structure in proteins. Despite the lack of theoretical methods, in addition to the IR absorption spectroscopy, various alternative experimental methods such as nonresonant and resonant Raman scattering spectroscopy, vibrational circular dichroism, and Raman optical activity have been extensively used to obtain complementary information on the secondary structure of a given polypeptide.[20−29] Recently, due to the advent of laser technology, a variety of novel spectroscopic tools, such as two-dimensional (2D) IR pump−probe and photon echo spectroscopies, have been developed and used to determine 3D structures of small polypeptides.[30−37] These 2D vibrational spectroscopic techniques have been shown to be successful in measuring various quantities such as vibrational coupling constants, angles between transition dipole vectors, etc., which are specifically dependent on the 3D structure of those small polypeptides such as trialanine[37] and acetylproline[35] in solutions. Furthermore, Woutersen and Hamm presented the 2D IR pump−probe spectra of the aqueous Fs helix solution, where the Fs helix is one of the best-known right-handed α-helix with 18 alanine and 3 arginine residues.[34] From the 2D difference spectrum experimentally measured, they were able to quantitatively determine the $A-E_1$ frequency splitting to be 10 cm^{-1}. Although by carrying out Monte Carlo (MC) simulations of the Fs helix system they could numerically calculate the 2D pump−probe spectra and compare them with experimental results, there still exist several issues that could not be resolved by their MC simulation studies. For example, the site-dependencies of the amide I local mode

* To whom correspondence should be addressed. Email address: mcho@korea.ac.kr.
[†] Sookmyung Women's University.
[‡] Korea University.

10.1021/jp048678e CCC: $27.50
Published on Web 05/29/2004

frequencies and their fluctuation amplitudes, hydrogen-bonding dynamics, local flexibility, delocalization of instantaneous amide I normal modes, spectral distributions of one- and two-exciton states, existence of *A*-like or E_1-like normal mode, distribution of transition dipole strength, etc., have not been fully elucidated yet. Furthermore, the asymmetric shape of the amide I IR band of α-helix in liquid water and two-dimensional line shapes of 2D IR signals for the parallel and perpendicular polarized pump and probe, and difference pump−probe spectra were not theoretically described yet.

Despite the existence of numerous different spectroscopic methods probing amide I vibrational dynamics, to interpret experimental results it is still necessary to have a theoretical model that is capable of quantitatively predicting both diagonal and off-diagonal Hessian matrix, in the amide I mode subspace, of a given polypeptide. Over the past few years, we have developed a systematic way to take into account the interpeptide as well as solute−solvent interaction effects on the amide I mode frequency shifts and vibrational coupling constants for various polypeptides ranging from a monopeptide like *N*-methylacetamide (NMA) to polypeptides with five peptide groups.[17,38−43] For instance, from the ab initio calculation studies of a number of NMA−water clusters, an extrapolation method for calculating the amide I mode frequency of an NMA dissolved in liquid water was developed[17] and used to quantitatively calculate the IR absorption spectrum[18] and 2D pump−probe spectra.[44] Furthermore, the same method was used to predict various 1D and 2D spectra of the NMA−methanol solution.[45] Overall, we found that the theory works quantitatively well in not only predicting solvation-induced frequency red-shifting behavior but also simulating 1D and 2D vibrational spectra in comparison to the experimental results. However, it is not automatically clear whether the same method in combination with quantum chemistry calculations is useful to theoretically determine amide I mode frequency shifts and coupling constants of lengthy polypeptides having more than 20 residues. Therefore, in the present paper, we will first provide evidence confirming the validity of the extrapolation method by carrying out semiempirical quantum chemistry calculations of various α-helical polyalanines. Then, the molecular dynamics simulation results of the aqueous α-helical polyalanine solution will be presented and discussed in detail in section III. Numerically calculated linear and nonlinear (2D) vibrational spectra will be presented in sections IV and V, respectively, and directly compared with experimental results. Finally, the main results and a few concluding remarks will be given in section VI.

II. Quantum Chemistry Calculation Results

The local amide I mode frequency was found to be determined by two distinctively different interactions, which are solute−solvent and interpeptide interactions. In the present section, we will focus on the latter type of interaction, and the solvatochromic frequency shift will be discussed in section III, where a molecular dynamics simulation method is employed to study amide I mode frequency fluctuation.

It was shown that the amide I local mode frequency is strongly dependent on the relative configurations of the neighboring peptides. To develop a model for quantitatively predicting the local amide I mode frequency, i.e., diagonal Hessian matrix elements, the electrostatic interaction between peptide groups was mainly considered and the transition and partial charges of the four sites, i.e., C(═O), O(═C), N(−H), and H(−N) atoms of a given peptide bond, were obtained by fitting ab initio calculation results of a variety of di- and tripeptides with a multivariate linear equation.[41,42] More specifically, the *m*th local amide I mode frequency in a given polypeptide can be estimated by calculating electrostatic potential field at the four sites of the *m*th peptide bond as

$$\tilde{\nu}_m = \tilde{\nu}_0 + \delta\tilde{\nu}_m^{\text{peptide}}$$

and

$$\delta\tilde{\nu}_m^{\text{peptide}} = \sum_{j=1}^{4} l_{j(m)}\phi_{j(m)}^{\text{peptide}} \quad (1)$$

where $\phi_{j_m}^{\text{peptide}}$ is the electrostatic potential at the *j*th site of the *m*th peptide bond and it is created by the partial charges of the other peptide groups around the *m*th peptide bond. The reference frequency, which is that of an isolated NMA molecule, was denoted as $\tilde{\nu}_0$ (= 1707 cm^{-1}). To quantitatively calculate $\tilde{\nu}_\text{m}$ values, one should have not only l_j values but also four partial charges of the four sites, i.e., O(═C), C(═O), N(−H), and H(−N). The four l_j values were obtained by using the multivariate least-squares fitting analysis of 96 *N*-methylacetamide−$n\text{D}_2\text{O}$ complexes and thus determined l_j values are l_O = −0.005 54, l_C = 0.0016, l_N = 0.004 79, and l_H = − 0.000 86.[41] Here, the dimension of l_j is a fraction of electronic charge, *e*. Now, using these l_j values, we determined the effective partial charges of the four sites of a given peptide group from the ab initio calculated local amide I mode frequencies for various di- and tripeptides, which were used as the reference data set, and the four partial charges were found to be c_O = − 0.871, c_C = 0.419, c_N = 0.793, and c_H = − 0.341.[42] To calculate the electrostatic potential, we used the dielectric constant to be 1. Again, the dimension of partial charge, c_j, is a fraction of electronic charge. The dimension of the electrostatic potential was converted into cm^{-1}/e. Although the extrapolation formula in eq 1 was found to be quantitatively reliable for short polypeptides as demonstrated in ref 43, we have not confirmed whether it is also valid for predicting amide I local mode frequencies of lengthy polypeptides such as a PA_N ($N \approx 20$), where *N* denotes the number of peptide bonds. The main goal of this section is to show that eq 1 is useful even for these cases of long α-helices, by carrying out a series of less expensive AM1 level calculations.[46]

A. Correlation between Structure and Amide I Mode Frequency. Recently, for a variety of polypeptides we have confirmed that the local amide I mode frequency is linearly proportional to the C═O bond length by using quantum chemistry calculation methods such as HF/6-311++G**.[43] However, the same method and basis set is very expensive and time-consuming to perform geometry optimization and vibrational analysis of a large α-helix with up to 20 peptide bonds. Thus, we have tried to find an alternative, effective, but quantitatively reliable method for such a purpose and found that the semiempirical AM1 model is useful. Although the structural properties, such as bond lengths, dihedral angles, etc., obtained by using the AM1 calculation method have known to be less accurate than other higher level ab initio calculation methods such as HF, MP2, and DFT, the structure−vibrational frequency relationship, i.e., amide I mode frequency vs C═O bond length, is still valid and in good agreement with the HF/6-311++G** results.

B. Hessian Matrix Reconstruction Analysis. Using the AM1 method, we carried out geometry optimization calculations and vibrational analyses of four α-helical PAs with N = 6, 10, 15, and 20, where both C- and N-terminals were capped by an

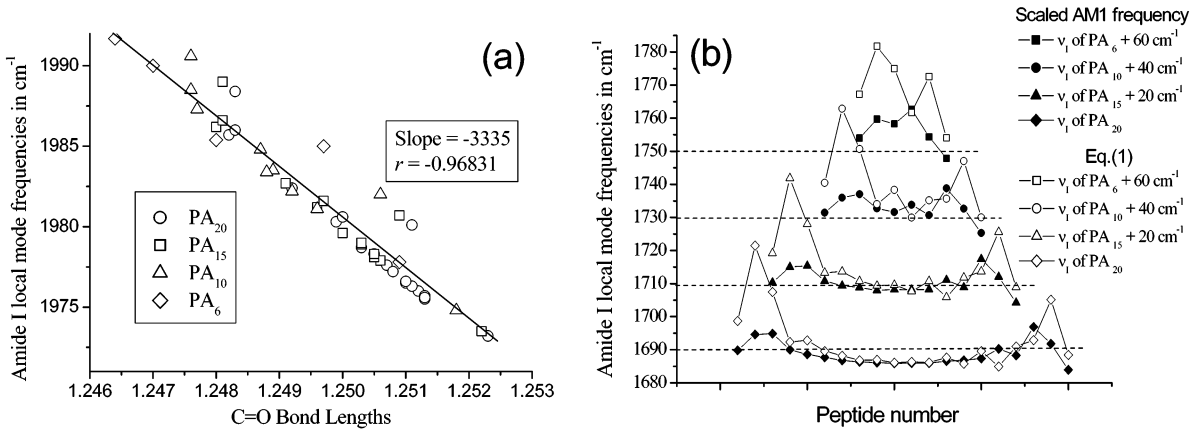

Figure 1. (a) Amide I local mode frequencies of PA_6, PA_{10}, PA_{15}, and PA_{20} obtained by using the Hessian matrix reconstruction method, AM1 geometry optimization, and vibrational analyses are plotted with respect to the C═O bond lengths. The vibrational frequencies are not scaled. (b) Local amide I mode frequencies of PA_6, PA_{10}, PA_{15}, and PA_{20} predicted by using the four-site model, eq 1, are compared with the scaled amide I local mode frequencies (see context for a detailed procedure on how to re-scale the AM1-calculated amide I frequency).

acetyl and methyl groups, respectively. From the AM1 vibrational analysis of each helical PA, one can obtain amide I normal-mode frequencies and corresponding eigenvectors. Now, using the so-called Hessian matrix reconstruction method developed by the authors recently,[41,42] N amide I local mode frequencies and vibrational coupling constants can be determined. In Figure 1a, thus calculated local amide I mode frequencies are plotted with respect to the C═O bond lengths, and the linear relationship between the two is clear—note that the amide I frequencies are not scaled. The best fit is $\tilde{\nu}_I^{AM1} = -3335 d_{C=O}^{AM1} + 6149\ cm^{-1}$. Here, the dimension of the C═O bond length is Å. The same linear relationship, though its slope is different from that in Figure 1a, was already found for a variety of small polypeptides, where the HF/6-311++G** method was employed. Therefore, even though it is well-known that the vibrational frequencies and molecular structures predicted by using AM1 calculations are not as reliable as those by HF/6-311++G** method, as long as the amide I mode frequency is concerned one can convert AM1-calculated amide I mode frequencies into those at the HF/6-311++G** level by using the linear relationship between $\tilde{\nu}_I$ and $d_{C=O}$.

Now, to show that the extrapolation method in eq 1 is useful even for long α-helices, in Figure 1b we plot the predicted amide I local mode frequencies (open squares, circles, triangles, and diamonds) by using eq 1 and scaled AM1-calculated amide I local mode frequencies (closed squares, circles, triangles, and diamonds), where the scaling factor is $\nu_{m=10}^{eq1}/\nu_{m=10}^{AM1}$ (for PA_{20}) = 0.8534. This factor is multiplied to all the AM1-calculated (unscaled) amide I local mode frequencies in Figure 1a. We found that eq 1 works well and predicts the general trend on the site-dependence of amide I local modes in a given α-helical PA, though it overestimates the local mode frequencies of the first three peptide groups. There are two possible explanations for the latter discrepancy. The first is that the four-site model, eq 1, with optimized parameters obtained from HF/6-311++G** calculations of small polypeptides ($N = 2-5$) is not sophisticated enough to describe the amide I local mode frequency shifts of the first three peptide groups in the N-terminus. The second is that the AM1-level calculations of C═O bond length and amide I normal-mode frequencies and eigenvectors are not sufficiently accurate. It is believed that the second is the reason for the notable failure of eq 1 in the region of the N-terminus because the four-site model was found to be reliable for predicting amide I local mode frequencies of short polypeptides with $N = 2-5$ but in contrast eq 1 works relatively poorly for PA_6 as can be seen in Figure 1b.[43] Nevertheless, the four-site model, eq 1, appears to be a far better method than any other previous theoretical model or ad hoc methods presented before and it is found to be an acceptable model for the longest PA, PA_{20}, considered in this subsection.

C. Chain Length Dependencies of Diagonal and Off-Diagonal Hessian Matrix Elements. For a short α-helical PA, the amide I local mode frequencies are highly site-dependent. As discussed in ref 42, the interpeptide interaction between two nearest neighboring peptide groups in a given α-helical polypeptide is repulsive so that the C═O bond length is shorter than that of an isolated peptide bond, which results in an increase of the amide I local mode frequency. More specifically, the two amide I local mode frequencies of a model tripeptide when its 3D conformation is an α-helix are larger than 1707 cm^{-1}, meaning that the interpeptide interaction induces blue shifts of the amide I local mode frequencies. This trend was found to be general as long as the target peptide group does not form any intramolecular hydrogen bond with other peptide groups. However, as the chain length increases, the peptide bond in the inner region of a lengthy α-helix will experience two competing interactions, i.e., blue-shifting interpeptide interactions with the two nearest neighboring peptide groups and red-shifting hydrogen-bonding interactions with ($j\pm4$)th peptide groups—note that a single intramolecular hydrogen-bonding interaction between 1 and 4 peptide bonds induces about a 20−30 cm^{-1} red-shift of the amide I mode frequency. Consequently, the local amide I mode frequencies of the peptides located in the inner region become rather insensitive to their positions in a given α-helical chain. These results suggest that one should not make a simple assumption that the diagonal Hessian matrix elements in the amide I subspace are identical when the segment in a given protein is in an α-helical conformation.

We next consider the vibrational coupling constants between neighboring peptides. As found in the recent quantum chemistry calculation studies on amide I vibrational couplings of various conformational short polypeptides,[42,43] the vibrational coupling constants were found to be almost independent of the chain length when the number of peptide bonds is less than six. This insensitivity of coupling constant with respect to the chain length is still valid even for longer polypeptides having up to 20 peptide bonds. The average 1−2, 1−3, and 1−4 coupling constants (in cm^{-1}) are found to be 5.35, −3.63, and −4.33, respectively, and the corresponding standard deviations are 1.67, 1.29, and 0.77 cm^{-1}, respectively. This again confirms the notion that the vibrational coupling constants do not depend on the chain length.

Before we close this section, we summarize the principal results from the semiempirical (AM1) calculation studies. The general trends, i.e., (1) the amide I local mode frequencies of the second and third peptide bonds from one of the two terminals are larger than the reference frequency of 1707 cm^{-1} and site-dependent and (2) the amide I local mode frequencies of the peptide groups in the inner region of a long PA are more or less independent of their positions, were found to be well-described by the extrapolation formula. Thus, it is believed that the main goal of the AM1 study, which is to show that the extrapolation method in eq 1 can be used to quantitatively describe the interpeptide-interaction-induced shifts of the amide I local modes in any α-helical PA, was achieved. In the following section, we will use this extrapolation method with the set of parameters $\{l_j\}$ and $\{c_j\}$ to numerically calculate the interpeptide-interaction-induced amide I mode frequency shifts of PA_{22} dissolved in liquid water.

III. Molecular Dynamics Simulation Results

To understand the structural fluctuation−spectra relationships of α-helices in liquid water, we will particularly consider the PA_{22} molecule, which was extensively studied experimentally and theoretically.[34,47−53] Recently, Hamm and co-workers carried out two-dimensional IR pump−probe spectroscopic studies of the Fs helix, which has 21 amino acid residues consisting of 18 alanines and three arginines.[34] Note that the arginine side chain has a positively charged group that can have hydrogen-bonding interactions with the polypeptide backbone. Furthermore, the side chain dynamics is rather slow so that one needs to run a very long MD simulation to fully take into account these slow processes. Therefore, we instead chose PA_{22} instead of Fs helix because there are no complicated side-chain effects on the amide I mode frequency fluctuation and on the conformational fluctuation of the polypeptide backbone as well as because PA_{22} is an ideal α-helix system that can be considered to be the reference system of all α-helical polypeptides.

A. MD Simulation Method. The constant-temperature molecular dynamics (MD) simulations were performed by using the SANDER module of the AMBER program package employing the parm99 force field.[54] The system consists of a single PA_{22} and 2192 TIP3P water molecules at neutral pH. Long-range electrostatic interactions are treated with the particle-mesh Ewald method implemented in the AMBER program.[55] The solvated system was subject to 1000 steps of conjugate gradient energy minimization and then brought into an equilibrium state for 100 ps at 273 K using the Berendsen coupling algorithm.[56] In all calculations, an 8.0 Å nonbonded interaction cutoff was used and nonboned pair lists were updated every 20 integration steps. The system was then coupled to an external heat bath with relaxation time of 0.1 ps. A 0.5 fs time step was used for the simulation. Structures were saved every 10 fs for detailed analyses. The simulation was performed for 2 ns. We also performed the same MD simulation for Fs helix in liquid water for 2 ns. However, within the 2 ns trajectory, in all aspects of statistics and dynamics we found little differences between Fs helix and PA_{22} solutions.

B. Structural Fluctuation and Hydrogen-Bonding Dynamics. *1. Dihedral Angle Fluctuation.* As the amide I local mode frequencies strongly depend on dihedral angles, ϕ_j and ψ_j, conformational fluctuation of the PA_{22} backbone and dynamics of surrounding water molecules are expected to considerably contribute to the overall frequency fluctuations. To this end, we first calculated average dihedral angles[57] $\langle\phi_j\rangle$ and $\langle\psi_j\rangle$ and their standard deviations, and they are plotted in parts a and b of Figure 2, respectively. The average dihedral angles of peptide bonds in the inner region of PA_{22} maintain their helical structures throughout the entire equilibrium simulation. Nevertheless, the average dihedral angles and their fluctuation amplitudes of peptide groups near the two terminals deviate from those values of peptide groups in the inner region. This indicates that the backbone structures near the two terminals are more flexible than those in the inner region.[53,58−60]

2. Hydrogen Bonding Dynamics. To study the hydration effect on each individual peptide C═O group, we first calculated the average number of water molecules forming a direct hydrogen bond with the peptide groups (see Figure 2c). Typically, one water molecule is involved in the hydrogen-bonding interaction with the carbonyl oxygen atom, whereas the number of water molecules hydrogen-bonded to the peptide groups near the C-terminus is larger than one—this means that those peptide groups are significantly exposed to solvent water. These observations are by no means surprising because the peptide bonds in the inner region form two strong hydrogen-bonds with $j\pm4$'th peptide groups though those near the C-terminus do not. A consequence of this distribution of hydrogen-bonding interaction strengths is that the dominant mechanism for solvatochromic amide I mode frequency shift is strongly dependent on the position of the target peptide bond in the PA_{22} chain.

C. Local Amide I Mode Frequency Fluctuation and Statistics: Aqueous PA_{22} Solution. *1. Local Amide I Mode Frequencies.* To numerically predict the solvation-induced amide I mode frequency shift, the following formula will be used

$$\delta\tilde{\nu}_{\mathrm{m}}^{\mathrm{water}}(t) = \sum_{j=1}^{4} l_j \phi_{j(m)}^{\mathrm{water}}(t) \tag{2}$$

where the four parameters, l_j, were already presented in section II. $\phi_{j(m)}^{\mathrm{water}}$ is the electrostatic potential at the jth site of the mth peptide bond, created by the partial charges of the surround water molecules. Here, the CHELPG partial charges of the deuterium and oxygen atoms of D_2O were calculated to be 0.412 and −0.824, respectively, at the HF/6-311++G** level.[17] The validity of the above method, eq 2, was extensively tested for various NMA−water clusters,[17] aqueous NMA solution,[18] and NMA dissolved in liquid methanol[45] by making direct comparisons of numerically predicted amide I IR absorption spectra and 2D IR pump−probe spectra with experimental results. Combining eq 1 with (2), the local amide I mode frequency of the mth peptide bond in an aqueous PA_{22} solution is given as

$$\tilde{\nu}_m(t) = \tilde{\nu}_0 + \delta\tilde{\nu}_m^{\mathrm{peptide}}(t) + \delta\tilde{\nu}_m^{\mathrm{water}}(t) \tag{3}$$

Note that the electrostatic potentials $\phi_{j(m)}^{\mathrm{peptide}}$ and $\phi_{j(m)}^{\mathrm{water}}$ fluctuates in time due to the conformational fluctuation and translational and rotational motions of the surrounding water molecules, respectively. In Figure 2d, the average amide I local mode frequencies, $\langle\tilde{\nu}_m\rangle$ for $m = 1-22$, are plotted (see closed circles). It is interesting to note that $\langle\tilde{\nu}_m\rangle$ values, except for the two peptide groups at each terminal, are almost constant regardless of its position. This is puzzling because we found that the amide I local mode frequencies of gas-phase PA molecules are strongly site-dependent as shown in Figure 2b. To theoretically explain this observation, we plot the values of $\tilde{\nu}_0 + \langle\delta\tilde{\nu}_m^{\mathrm{peptide}}\rangle$ and $\tilde{\nu}_0 + \langle\delta\tilde{\nu}_m^{\mathrm{water}}\rangle$ separately, which correspond to the cases where either interpeptide interaction or solvation interaction effect is only considered (see open squares and open triangles in Figure 2d, respectively). Note that the interpeptide-interaction-induced effect on the amide I local mode frequencies

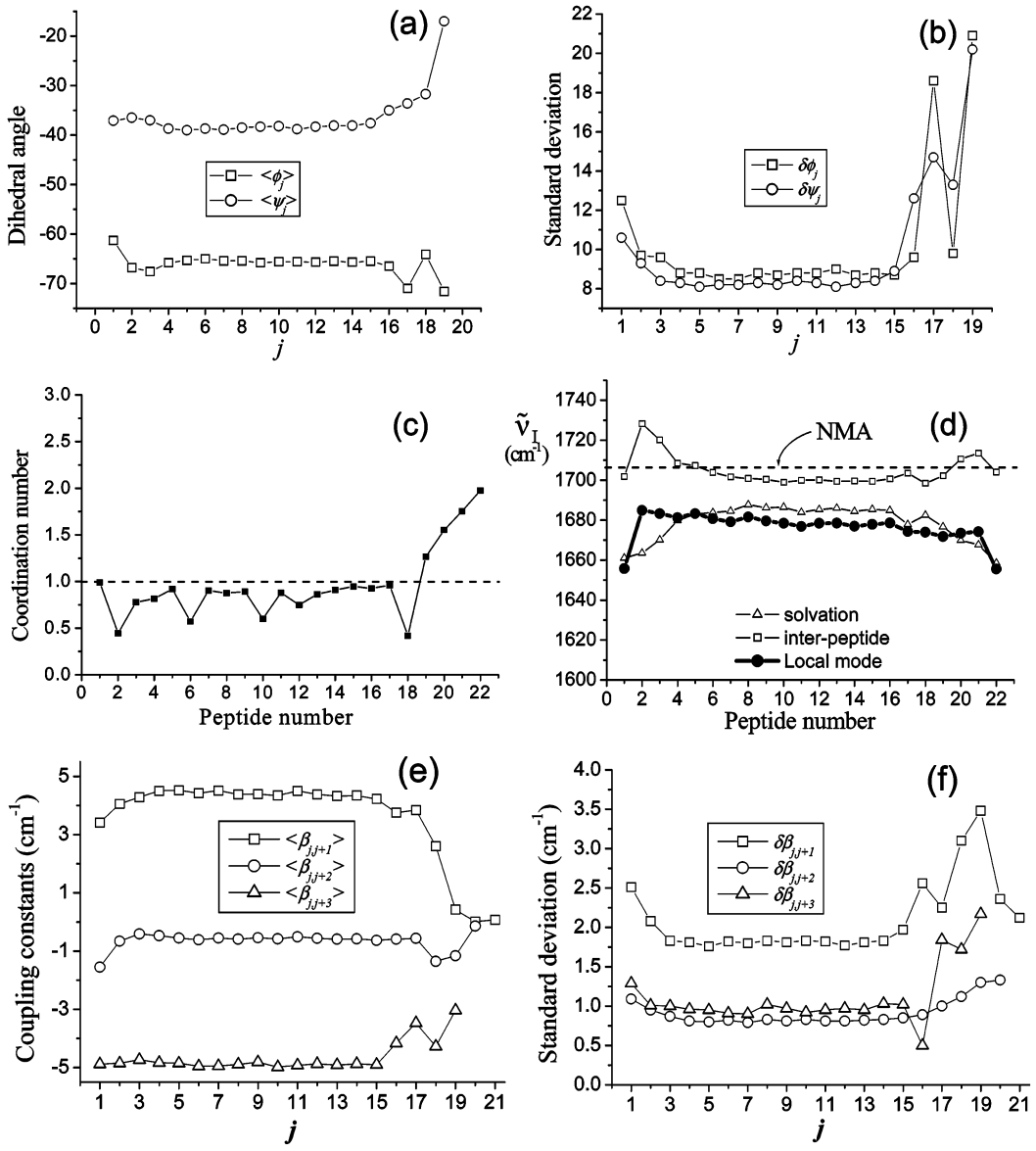

Figure 2. (a) Plots of ensemble-averaged dihedral angles $\langle\phi_j\rangle$ and $\langle\psi_j\rangle$ and (b) their standard deviations, $\delta\phi_j$ and $\delta\psi_j$. (c) Plots of average numbers of hydrogen-bonded water molecules to each carbonyl oxygen atom. (d) Plots of ensemble-averaged frequencies, $\langle\tilde{\nu}_m(t)\rangle$, $\tilde{\nu}_0 + \langle\delta\tilde{\nu}_m^{peptide}(t)\rangle$, and $\tilde{\nu}_0 + \langle\delta\tilde{\nu}_m^{water}(t)\rangle$. (e) Plots of average coupling constants $\langle\beta_{j,j+1}\rangle$, $\langle\beta_{j,j+2}\rangle$, and $\langle\beta_{j,j+3}\rangle$ and (f) the standard deviations $\delta\beta_{j,j+1}$, $\delta\beta_{j,j+2}$, and $\delta\beta_{j,j+3}$.

is to make them blue-shifted and identical to the case of an isolated PA molecule studied in section II. However, as can be seen in the plot of $\tilde{\nu}_0 + \langle\delta\tilde{\nu}_m^{water}\rangle$ (see open triangles in Figure 2d), the magnitude of the solvatochromic amide I local mode frequency shift is negatively large as the location of the peptide group is close to the two terminals, whereas those of peptide groups in the inner region are rather small. This trend is in accord with the hydrogen-bonding statistics found in the above subsection. Consequently, the two contributions, i.e., blue-shifting interpeptide-interaction-induced frequency shift and red-shifting hydration-induced frequency shift, are added together to make the amide I local mode frequencies rather independent to their positions in the PA_{22} chain.

2. Vibrational Coupling Constants. Due to the conformational fluctuation of the PA_{22} in liquid water, the distance and relative orientation between any pair of peptide groups also fluctuate in time. As discussed in ref 42, the coupling constant $\beta_{j,j\pm1}$ between any two nearest neighboring peptides should be obtained from the high-level ab initio calculation result of glycine dipeptide analogue. On the other hand, the long-range coupling constants such as $\beta_{j,j\pm k}$ with $k > 1$ can be determined by using the transition dipole coupling model developed by Krimm and co-workers.[3−6] Now, from the MD trajectories, we calculated the average coupling constants, denoted as $\langle\beta_{j,j+k}\rangle$ for $k = 1-3$, and the corresponding standard deviations, $\delta\beta_{j,j+k}$ (see parts e and f of Figure 2, respectively). The coupling constants $\langle\beta_{j,j+k}\rangle$ are almost independent of j and $\langle\beta_{j,j+1}\rangle$ is quantitatively similar to $-\langle\beta_{j,j+3}\rangle$, though $\langle\beta_{j,j+2}\rangle$ values are significantly small. The standard deviation of $\beta_{j,j+1}$ is almost twice as large as those of $\beta_{j,j+2}$ and $\beta_{j,j+3}$. Note that the magnitude of $\delta\beta_{j,j+1}$ is a measure of the local flexibility around the jth peptide bond so that the large values of $\delta\beta_{j,j+1}$ near the two terminals in comparison to $\delta\beta_{9,10}$ are expected and observed in the present calculation. In sections IV and V, these distributions of the amide I vibrational frequencies and coupling constants will be used to numerically calculate the linear and nonlinear vibrational spectra of PA_{22} in liquid water.

Using the procedure outlined above, one can obtain the diagonal and off-diagonal Hamiltonian matrix elements, i.e.,

$$H_1(t) = \begin{bmatrix} \tilde{\nu}_1(t) & \beta_{1,2}(t) & \beta_{1,3}(t) & \cdots & \beta_{1,N}(t) \\ \beta_{1,2}(t) & \tilde{\nu}_2(t) & \beta_{2,3}(t) & \cdots & \beta_{2,N}(t) \\ \beta_{1,3}(t) & \beta_{2,3}(t) & \tilde{\nu}_3(t) & \cdots & \beta_{3,N}(t) \\ \vdots & \vdots & \vdots & \ddots & \vdots \\ \beta_{1,N}(t) & \beta_{2,N}(t) & \beta_{3,N}(t) & \cdots & \tilde{\nu}_N(t) \end{bmatrix} \quad (4)$$

From the above one-exciton Hamiltonian, one can obtain both eigen-frequencies and eigenvectors associated with the instantaneous amide I normal modes at time t. In the following sections, both dynamical and statistical behaviors of the local and normal amide I mode frequencies will be discussed in detail.

D. Correlation Functions of Local Amide I Mode Frequencies. Although the equilibrium vibrational properties, ensemble-averaged local mode frequencies, and vibrational coupling constants were presented above, yet another piece of critical information required in the calculations of vibrational spectra is their dynamics. Not only the diagonal but also off-diagonal Hessian matrix elements fluctuate over time, and their correlation times are strongly related to the time scales of structural fluctuation and solute−solvent dynamics. We calculated the following time correlation functions of amide I local mode frequencies

$$C_m(t) = \langle \{\tilde{\nu}_m(t) - \langle \tilde{\nu}_m \rangle\} \{\tilde{\nu}_m(0) - \langle \tilde{\nu}_m \rangle\} \rangle \quad (5)$$

and particularly two of them, $C_{m=10}(t)$ and $C_{m=20}(t)$, which represent the middle and terminal peptide groups, are plotted in parts a and b of Figure 3, respectively. It should be noted that, although all 22 correlation functions are not plotted in the present paper, they all exhibit strongly bimodal decaying patterns. The ultrafast component decays within a few picoseconds, but the slowly decaying component is very slow in comparison to the experimental time scale—note that the time-resolved 2D IR pump−probe spectra were obtained for every 1 ps up to 4 ps.[34] To elucidate the origins of these two distinctively different components, we rewrite eq 5 as

$$C_m(t) = \langle \{\delta\delta\tilde{\nu}_m^{\text{peptide}}(t) + \delta\delta\tilde{\nu}_m^{\text{water}}(t)\} \{\delta\delta\tilde{\nu}_m^{\text{peptide}}(0) + \delta\delta\tilde{\nu}_m^{\text{water}}(0)\} \rangle$$

$$= C_m^{\text{peptide}}(t) + C_m^{\text{water}}(t) + C_m^{\text{peptide-water}}(t) \quad (6)$$

where

$$\delta\delta\tilde{\nu}_m^{\text{peptide}}(t) = \delta\tilde{\nu}_m^{\text{peptide}}(t) - \langle \delta\tilde{\nu}_m^{\text{peptide}}(t) \rangle$$

$$\delta\delta\tilde{\nu}_m^{\text{water}}(t) = \delta\tilde{\nu}_m^{\text{water}}(t) - \langle \delta\tilde{\nu}_m^{\text{water}}(t) \rangle$$

$$C_m^{\text{peptide}}(t) = \langle \delta\delta\tilde{\nu}_m^{\text{peptide}}(t)\delta\delta\tilde{\nu}_m^{\text{peptide}}(0) \rangle$$

$$C_m^{\text{water}}(t) = \langle \delta\delta\tilde{\nu}_m^{\text{water}}(t)\delta\delta\tilde{\nu}_m^{\text{water}}(0) \rangle$$

$$C_m^{\text{peptide-water}}(t) = 2\langle \delta\delta\tilde{\nu}_m^{\text{peptide}}(t)\delta\delta\tilde{\nu}_m^{\text{water}}(0) \rangle \quad (7)$$

The total correlation function $C_m(t)$ is divided into three parts, correlation function of interpeptide interaction-induced frequency fluctuation, correlation function of hydration-induced frequency fluctuation, and cross correlation function. The mean square fluctuation amplitudes, $C_m(0)$ for $m = 1-22$, are more or less constant of 250 cm^{-2} and independent of m, though $C_m^{\text{peptide}}(0)$, $C_m^{\text{water}}(0)$, and $C_m^{\text{peptide-water}}(0)$ are strongly dependent on where the peptide bond is in the chain. In Figure 3, these three contributions to $C_m(t)$ are separately plotted for $m = 10$ and 20. It is interesting to note (1) that the decaying pattern of $C_m(t)$ is largely determined by $C_m^{\text{water}}(t)$, (2) that both $C_m^{\text{peptide}}(t)$ and $C_m^{\text{peptide-water}}(t)$ contain very slowly decaying component that is associated with the conformational fluctuation of the PA_{22} backbone structure, (3) that the two contributions from $C_m^{\text{peptide}}(t)$ and $C_m^{\text{peptide-water}}(t)$ cancel out with each other, and (4) that the large amplitudes of $C_{20}^{\text{peptide}}(t)$ and $C_{20}^{\text{peptide-water}}(t)$ in comparison to those of the inner peptide bond ($m = 10$) are found to be related to the local flexibility of the 20th peptide group near the C-terminus. The ultrafast (subpicosecond) relaxation of $C_m^{\text{water}}(t)$ originates from the solvation dynamics of water such as librational (hindered rotational) motions.[18] In addition, the fast decaying component in $C_m^{\text{peptide}}(t)$ is associated with fluctuations induced by various (intramolecular) amide vibrations that modulate the amide I vibrational mode frequencies. On the basis of the above calculations, even though there exist ultrafast decaying components in the correlation functions of the amide I local mode frequency fluctuations, its amplitude is relatively small and the slowly decaying component is very slow in comparison to the time scales of vibrational dynamics and experiments (approximately a few picoseconds). Therefore, the line-broadening process can be approximately described by considering the inhomogeneous distributions of instantaneous normal-mode frequencies.

E. Instantaneous Normal-Mode (INM) Analysis: INM Spectrum and Delocalization. Before we present numerically calculated IR absorption and 2D vibrational spectra, there are a few important issues that require clarification. In the case of PA_{22} in liquid water, unlike a small rigid molecule, the amide I normal modes calculated from each instantaneous configuration of PA_{22} are poorly defined. In other words, the eigenvector matrixes change in time constantly and one cannot make a one-to-one correspondence between two normal modes obtained from two different snapshot configurations separated in time. Consequently, the concept of polypeptide normal mode, in a conventional way, is not useful for calculating vibrational spectra of polypeptides in solution. The same situation was also found in the short-time description of liquid dynamics and the instantaneous normal-mode analyses were performed for a variety of neat liquids and solutions and found to be useful in describing ultrafast solvation dynamics, IR and Raman responses, etc.[61−64]

Now, diagonalizing the instantaneous Hessian matrixes obtained from the MD simulation, one can calculate the *instantaneous* amide I normal-mode frequencies and corresponding eigenvectors. In Figure 4a, we plot the calculated INM spectrum, which is the density of state (DOS) of the one-exciton band, defined as

$$\rho_1(\omega) = \frac{1}{N}\langle \sum_{\alpha} \delta(\omega - \omega_\alpha) \rangle \quad (8)$$

where the angle bracket represents the ensemble average over the instantaneous configurations sampled from the MD trajectory. $\rho_1(\omega)$ appears to be asymmetric. We will use this INM (DOS of one-exciton band) spectrum for the calculation of the linear and nonlinear vibrational spectra in the following sections.

Using the corresponding eigenvector elements obtained from each individual instantaneous configuration, one can calculate the inverse participation ratio (IPR) that provides information on the number of amide I local modes participating in a given normal mode. For a given instantaneous Hamiltonian matrix at

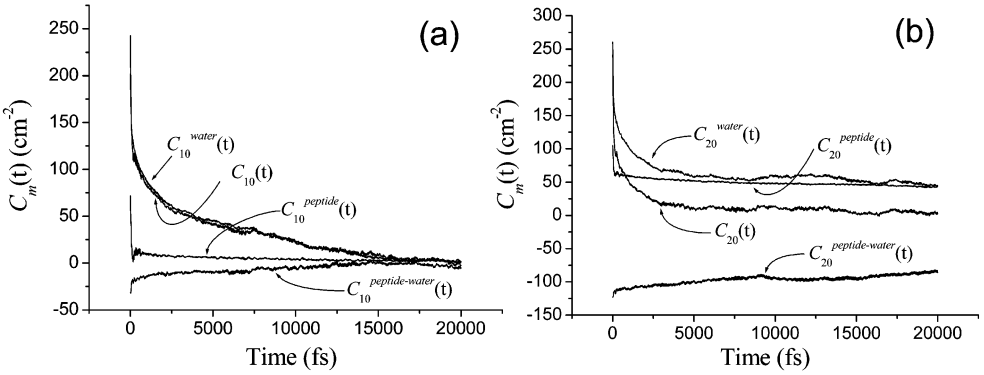

Figure 3. Correlation functions of fluctuating amide I local mode frequencies of the 10th and 20th peptide groups. The three different contributions (see the context) to the total correlation function are also plotted.

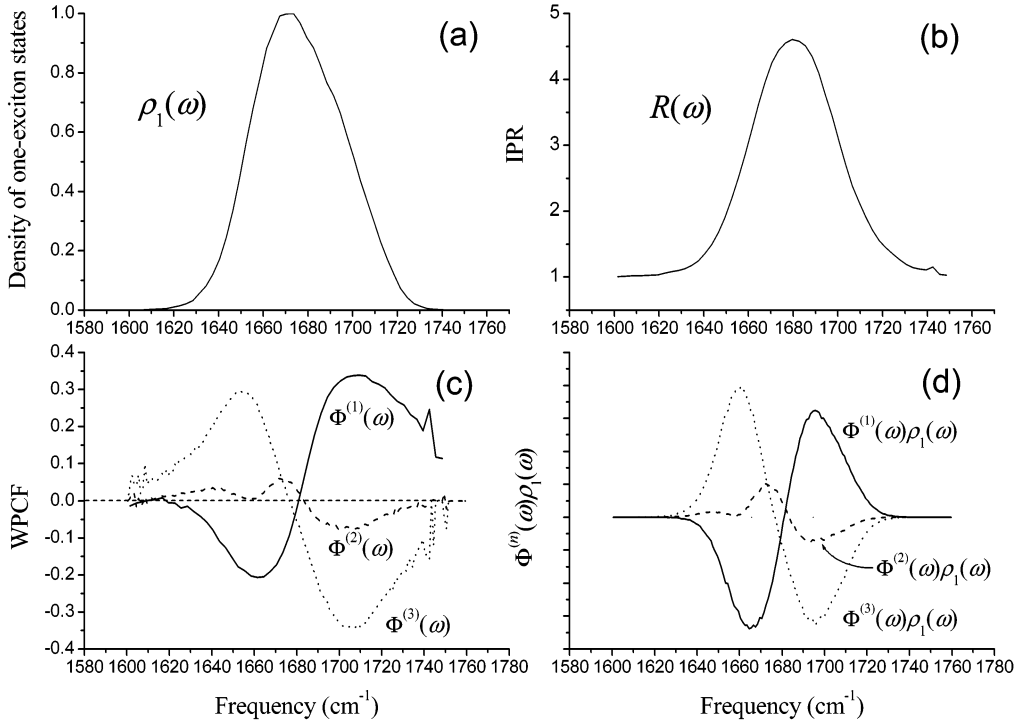

Figure 4. (a) Density of one-exciton states, $\rho_1(\omega)$. (b) Inverse participation ratio spectrum, $R(\omega)$. (c) Weighted phase-correlation factor spectrum, $\Phi(\omega)$. (d) Product of WPCF and density of one-exciton states spectra, i.e., $\Phi(\omega)\rho_1(\omega)$.

time t, the IPR of the αth instantaneous normal mode can be calculated by

$$\mathrm{IPR}_\alpha \equiv \left(\sum_j U_{\alpha,j}^4\right)^{-1} \tag{9}$$

where $U_{\alpha,j}$ is the jth element of the eigenvector associated with the αth amide I normal mode. In Figure 4b, the calculated IPR spectrum defined as

$$R(\omega) \equiv N^{-1}\left\langle \sum_\alpha \left(\sum_j U_{\alpha,j}^4\right)^{-1} \delta(\omega - \omega_\alpha)\right\rangle / \rho_1(\omega)$$

is plotted. The IPR value is typically less than 5, meaning that all instantaneous amide I normal modes are highly localized onto just a few local modes. It is clear that this localization process is induced by the conformational fluctuation and diagonal and off-diagonal disorders of the one-exciton Hamiltonian matrix. It is also interesting to note that the shape of $R(\omega)$ is a Gaussian with the center at 1680 cm^{-1} and the width of 37 cm^{-1}.

F. Phase Correlation between Neighboring Local Modes. Although the extent of delocalization of each individual INM could be quantitatively estimated by examining the IPR spectrum, $R(\omega)$, in Figure 4b, there is another critical issue on the phase relationship between different local amide I modes in a given normal mode. Over the years, it has been believed that the amide I normal modes of a lengthy α-helix can be classified into two distinctively different types of vibrations, i.e., *A*-mode-like and E_1-mode like. The *A*-mode-like normal mode refers to the normal mode having all eigenvector elements the same signs (in-phase). On the other hand, the signs of the eigenvector elements of the E_1-mode-like normal mode are alternating, meaning that the eigenvector elements of nearest neighboring local amide I modes are out-of-phase with each other. On the basis of this notion, there have been numerous attempts to quantitatively determine the frequency splitting between these two types of normal modes.[65,66] However, because the diagonal Hessian matrix elements could not be accurately determined for any lengthy polypeptides *in solutions*, it was not possible to directly address the issue on the existence of these *A*- or E_1-like amide I modes of the aqueous α-helix

solution. As can be seen in Figure 4b, due to the localized nature of the instantaneous amide I normal modes, there is no such an ideal *A*-mode nor E_1-mode in reality. Nevertheless, one can still make an argument that, by carefully examining the eigenvector elements of all INMs, the amide I normal modes are rather close to *A*-mode-like instead of E_1-mode-like, and vice versa. To quantitatively address this issue, we propose that the following quantity, $P_\alpha^{(n)}$, named as the weighted phase-correlation factor (WPCF), can serve as a measure of how close a given normal mode is to *A*-mode-like or to E_1-mode-like

$$P_\alpha^{(n)} \equiv \sum_{j=1}^{N-n} \mathrm{sign}(U_{\alpha,j}U_{\alpha,j+n})|U_{\alpha,j}U_{\alpha,j+n}| \qquad (10)$$

where $\mathrm{sign}(U_{\alpha,j}U_{\alpha,j+n})$ is either $+1$ or -1 depending on the sign of the product $U_{\alpha,j}U_{\alpha,j+n}$.

Before we present the calculation result using eq 10, let us consider a few limiting cases to understand the physical meaning of the WPCF defined in eq 10. First of all, consider the case when $n = 1$. In this case, $P_\alpha^{(1)}$ is approximately a measure of weighted phase-correlation between any pair of eigenvector elements of two nearest neighboring peptides. In the extreme case that a given INM is completely delocalized all over the N peptide groups and also it is purely *A*-mode-like, $U_{\alpha,j}$ for all j equals to $1/\sqrt{N}$ and then the WPCF value $P_\alpha^{(1)}$ becomes $1 - {}^1/_N$. Thus, the upper bound of WPCF $P_\alpha^{(1)}$ is 1. On the other hand, in the other extreme case that the INM is completely delocalized and E_1-mode-like, $U_{\alpha,j}$ for all j equals to $(-1)^j/\sqrt{N}$ and the WPCF value $P_\alpha^{(1)}$ is $-1 + {}^1/_N$, which suggests that the lower bound of WPCF $P_\alpha^{(1)}$ is -1. Now, consider the case that the normal mode is completely localized on the jth amide I local mode so that $U_{\alpha,j} = 1$ and $U_{\alpha,k} = 0$ (for $k \neq j$). In this case, the WPCF value $P_\alpha^{(1)}$ becomes zero. Therefore, on the basis of the above analysis, we found that the $P_\alpha^{(1)}$ value can provide two important pieces of information, e.g., both the extent of delocalization and the phase-relationship of eigenvector elements of two nearest neighboring amide I local vibrations. Similarly, $P_\alpha^{(2)}$ gives us information on the weighted phase-correlation between a pair of eigenvector elements of the jth and $(j + 2)$th peptide groups. Other than $P_\alpha^{(1)}$, one should pay attention to the value of $P_\alpha^{(3)}$ because the vibrational coupling constant $\beta_{j,j\pm3}$ between the jth and $(j + 3)$th peptide groups is as large as $\beta_{j,j\pm1}$ due to the intramolecular hydrogen-bonding interaction between the two (see Figure 2e). Thus, $P_\alpha^{(3)}$ for the αth INM provides information on the weighted phase-correlation between $U_{\alpha,j}$ and $U_{\alpha,j+3}$ (for all j).

Then, taking the ensemble average, one can obtain the WPCF spectra defined as $\Phi^{(n)}(\omega) \equiv \mathrm{N}^{-1}\langle\sum_\alpha \mathrm{P}_\alpha^{(n)}\delta(\omega - \mathrm{T}\omega_\alpha)\rangle/\rho_1(\omega)$ and for $n = 1-3$ we plot them in Figure 4c. The other cases of $\Phi^{(n)}(\omega)$ for $n > 3$ are not plotted here and they are not important because, due to the small coupling constants $\beta_{j,j\pm n}$ (for $n > 3$), those peptide groups separated far apart along the helical chain do not strongly participate in a given normal mode. Now, let us consider the WPCF spectrum of $n = 1$, $\Phi^{(1)}(\omega)$, in Figure 4c. Interestingly, the $\Phi^{(1)}(\omega)$ spectrum is divided into two parts with the boundary at 1680 cm^{-1}. The WPCF values of normal modes of which frequencies are less than 1680 cm^{-1} are negative whereas those of which frequencies are larger than 1680 cm^{-1} are positive. This $\Phi^{(1)}(\omega)$ spectrum suggests that the low-frequency INMs can be assigned to the E_1-like modes and the high-frequency normal modes are *A*-like modes—note that the same pattern was also observed for a model dipeptide, that is to say, the symmetric amide I normal-mode frequency of the di-peptide in its right-handed α-helical conformation is about 10−20 cm^{-1} larger than that of the asymmetric normal mode.[41] Therefore, if $\Phi^{(1)}(\omega)$ spectra were only taken into consideration, one might reach a conclusion that the high-frequency amide I INMs are *A*-mode-like and the low-frequency modes are E_1-mode-like. However, one can make a different conclusion by carefully examining the $\Phi^{(3)}(\omega)$ spectrum—note that the $\Phi^{(2)}(\omega)$ spectrum fluctuates around 0, meaning that any pair of peptide groups separated by one peptide do not strongly couple to each other as can be expected from the small $\beta_{j,j\pm2}$ values. Again, the $\Phi^{(3)}(\omega)$ spectrum is divided into two parts much like the $\Phi^{(1)}(\omega)$ spectrum. However, in the case of $\Phi^{(3)}(\omega)$ the higher frequency (>1680 cm^{-1}) modes are E_1-mode-like whereas the lower frequency (<1680 cm^{-1}) modes are *A*-mode-like. This is exactly the opposite conclusion in comparison to that from the $\Phi^{(1)}(\omega)$ spectrum. From these detailed analyses of eigenvectors and phase-correlations, can we make any conclusive statement on the existence of *A*-like or E_1-like amide I modes in the α-helix in liquid water? It is believed that the conceptual classification of *A*-mode-like and E_1-mode-like needs to be specified as demonstrated above. If one were interested in phase correlation between two *nearest* neighboring amide I local vibrations, we found that the high (low) frequency NMs are rather close to *A*-(E_1-)mode-like. On the other hand, if one were interested in that between jth and $(j + 3)$th amide I local vibrations, one might reach a conclusion that the high (low) frequency NMs are rather close to E_1-(*A*-)mode-like. Conclusively, there is no unique way to classify a given NM to be either *A*-mode-like or E_1-mode-like.

To roughly estimate the $A-E_1$ frequency splittings, we plot the products of $\rho_1(\omega)$ and WPCF spectra, i.e., $\Phi^{(n)}(\omega)\rho_1(\omega)$ for $n = 1-3$, in Figure 4d. In this figure, the $A-E_1$ frequency splitting from the $\Phi^{(1)}(\omega)$ spectrum is estimated to be 30 cm^{-1}, whereas that from the $\Phi^{(3)}(\omega)$ spectrum is to be -33 cm^{-1}. Here, it should be noted that the $A-E_1$ frequency splitting was measured to be 10 cm^{-1} by Hamm and co-workers by using the two-dimensional IR pump−probe spectroscopy, though they considered the Fs-helix instead of α-helical polyalanine in liquid water.[34] However, as will be discussed in section V, their method of obtaining difference spectrum is to some extent arbitrary so that their value of 10 cm^{-1} is a bit questionable and cannot be directly compared with the present calculation results.

IV. Linear Absoprtion Spectrum

To calculate the one-dimensional IR absorption spectrum, we will use the INM analysis method. That is to say, the permanent dipole moment of the PA_{22} is linearly expanded with respect to the instantaneous normal coordinates. Then, the dipole−dipole correlation function associated with amide I vibrations can be approximated to be

$$\langle\mu_1(t)\mu_1(0)\rangle \cong \left\langle \sum_\alpha \left|\left(\frac{\partial\mu}{\partial Q_\alpha}\right)_0\right|^2 Q_\alpha(t)Q_\alpha(0)\right\rangle \qquad (11)$$

where $\mu_1(t)$ is the time-dependent dipole moment of the amide I vibrations and Q_j denotes the jth instantaneous normal coordinate. In the harmonic approximation, the autocorrelation function of harmonic oscillator coordinate is simply given as $\langle Q_\alpha(t)Q_\alpha(0)\rangle = \langle Q_\alpha^2\rangle \cos\omega_\alpha t = (k_BT/M_\alpha\omega_\alpha^2)\cos\omega_\alpha t$. Furthermore, by noting that the normal-mode frequencies are in a rather narrow range from 1640 to 1720 cm^{-1} (see Figure 4a), eq 11 can be approximately written as

$$\left\langle \sum_{\alpha} \left| \left(\frac{\partial \mu}{\partial Q_{\alpha}} \right)_0 \right|^2 \cos \omega_{\alpha} t \right\rangle \tag{12}$$

Then, the IR absorption spectrum, which is linearly proportional to the Fourier transform of the above dipole−dipole correlation function, is given as

$$I(\omega) \sim \left\langle \sum_{\alpha} \left| \left(\frac{\partial \mu}{\partial Q_{\alpha}} \right)_0 \right| \right\rangle^2 \delta(\omega - \omega_{\alpha}) \tag{13}$$

From the instantaneous configurations, we calculated the ensemble average of the transition dipole strength, $|(\partial\mu/\partial Q_{\alpha})_0|^2$, and the corresponding transition dipole strength spectrum, denoted as $D(\omega)$ ($\equiv I(\omega)/\rho_1(\omega)$) is plotted in Figure 5a. Interestingly, the transition dipole strengths of the high-frequency (>1680 cm^{-1}) INMs are smaller than those of the low-frequency (<1680 cm^{-1}) INMs. This can be explained by examining the WPCF spectra in Figure 4c. Suppose that the INMs are strongly localized on two nearest neighboring peptide groups. Then, as can be seen in the $\Phi^{(1)}(\omega)$ spectrum, the phases of the two eigenvector elements of one of the high-frequency INMs are identical. Then, the transition dipole of the NM is given as a linear combination of two local mode transition dipoles with the weighting factors having the same signs. In this case, much like the dipeptide in an α-helical conformation, the transition dipole strength of the *A*-like mode (or symmetric stretching mode in the case of a dipeptide) is larger than that of the E_1-like mode (or asymmetric stretching mode in the case of a dipeptide). However, the numerically calculated transition dipole strength, $D(\omega)$, exhibits the opposite trend and cannot be explained by using the $\Phi^{(1)}(\omega)$ spectrum. On the other hand, this puzzling trend of $D(\omega)$ can be explained by considering the $\Phi^{(3)}(\omega)$ spectrum. We will omit any further discussion along this line and leave it to the readers, but these results suggest that the transition dipole strength is largely dictated by the delocalization over two local modes forming a direct intramolecular hydrogen bond to each other.

Now, the IR absorption spectrum can then be obtained by multiplying the transition dipole strength spectrum $D(\omega)$ and INM spectrum, $\rho_1(\omega)$, given in Figure 4a. The resultant IR spectrum based on the INM analysis is shown in Figure 5b. Although the distribution of fundamental transition frequencies was properly taken into account in the above numerical calculation, the vibrational dephasing contribution to the linear absorption spectrum was not. Therefore, one can replace the Dirac delta function in eq 13 with a Lorentzian function as

$$I(\omega) \sim \left\langle \sum_{\alpha} \left| \left(\frac{\partial \mu}{\partial Q_{\alpha}} \right)_0 \right|^2 \frac{\gamma_{\alpha}}{(\omega - \omega_{\alpha})^2 + \gamma_{\alpha}^2} \right\rangle \tag{14}$$

where the dephasing constant of the αth INM was denoted as γ_{α}. Although γ_{α} of each individual normal mode can be a function of its frequency, we will assume that the dephasing constants of all INMs are identical and constant to be 8 cm^{-1} throughout this paper—the dephasing constant of 8 cm^{-1} is obtained by fitting to experiment as discussed below. In Figure 5b, the broadened $I(\omega)$ is also plotted and the line shape is found to be quantitatively close to the experimentally measured $I(\omega)$ for Fs-helix in ref 34. Also, it is noted that $I(\omega)$ is slightly asymmetric and its line shape is neither Gaussian nor Lorentzian, which is also similar to the experiment. This asymmetric line shape of an α-helix in solution has not been clarified before, but now it becomes clear that it originates from (1) the asymmetric distribution of amide I normal-mode frequencies (Figure 4a) and (2) nonuniform distribution of the transition dipole strengths with respect to the INM frequencies (Figure 5a).

V. Two-Dimensional Infrared Pump-Probe Spectra

Although the one-dimensional IR absorption spectrum numerically calculated was compared with experiment and the two were found to be quantitatively in good agreement with each other, the more stringent test of the present calculation method would be to make direct comparisons of numerically calculated 2D IR pump−probe spectra with experimental results of Hamm and co-workers.[34] Although they carried out 2D IR pump−probe experiment for the Fs-helix not polyalanine, as mentioned in section III-A we found that there is little difference in the MD simulation results of α-helical polyalanine and Fs-helix.

A. Two-Exciton States. To calculate three distinctively different contributions, stimulated emission, ground-state bleaching, and transient absorption, to the 2D IR pump−probe response functions, it is necessary to consider two-exciton states, where we assumed that the overtone anharmonicity of each local amide I mode is 16 cm^{-1} and that the anharmonicities of combination modes are used to be 1 cm^{-1} to fit the experimental spectra in ref 34. Now, the ensemble-averaged, normalized density of two-exciton states can be calculated by

$$\rho_2(\omega) = \frac{2}{N(N+1)} \left\langle \sum_{f} \delta(\omega - \omega_f) \right\rangle \tag{15}$$

where the summation is over all two-exciton states obtained by diagonalizing each instantaneous two-exciton Hamiltonian. The calculated $\rho_2(\omega)$ is plotted in Figure 6a. Unlike the case of one-exciton band, the DOS of the two-exciton band $\rho_2(\omega)$ is symmetric and close to a Gaussian function. To understand the one-quantum excitation profile from the one-exciton band to the two-exciton band, we calculate the ensemble-averaged, normalized two-dimensional transition spectral density (see Figure 6b) defined as

$$\bar{\rho}(\omega_E,\omega_F) = \frac{2}{N^2(N+1)} \left\langle \sum_{e} \sum_{f} \delta(\omega_E - \omega_e) \delta(\omega_F - \omega_f) \right\rangle \tag{16}$$

where the summations over *e* and *f* are all over the one- and two-exciton states, respectively. From the definition of $\bar{\rho}(\omega_E,\omega_F)$, it can be viewed as a 2D joint probability density. On the basis of direct comparative investigation, we found that the numerically calculated $\bar{\rho}(\omega_E,\omega_F)$ is quantitatively similar to the product of $\rho_1(\omega)$ and $\rho_2(\omega)$, i.e., $\bar{\rho}(\omega_E,\omega_F) \cong \rho_1(\omega_E)\rho_2(\omega_F)$. This result suggests that the probability of finding a one-exciton state with frequency of ω_E is not correlated with the probability of finding a two-exciton state with frequency of ω_F. Next, let us consider the 2D spectral distribution of dipole strength associated with transitions from $|e>$ to $|f>$, which is defined as

$$\bar{D}(\omega_E,\omega_F) \equiv \frac{2\left\langle \sum_{e} \sum_{f} |\mu_{ef}(\omega_e,\omega_f)|^2 \delta(\omega_E - \omega_e) \delta(\omega_F - \omega_f) \right\rangle}{N^2(N+1)\bar{\rho}(\omega_E,\omega_F)} \tag{17}$$

In Figure 6c, $\bar{D}(\omega_E,\omega_F)$ thus calculated is plotted. The transition dipole strengths between low-frequency one-exciton state to low-frequency two-exciton state and between high-frequency one-exciton state to high-frequency two-exciton state are relatively large. However, the more relevant spectrum is

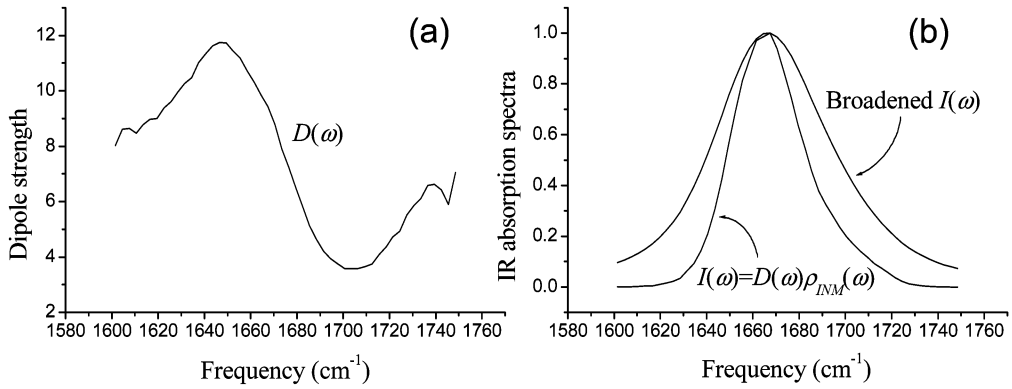

Figure 5. (a) IR dipole strength spectrum, $D(\omega)$. (b) INM-calculated IR absorption spectrum, $\rho_1(\omega)D(\omega)$, and broadened spectrum with dephasing constant of 8 cm^{-1}.

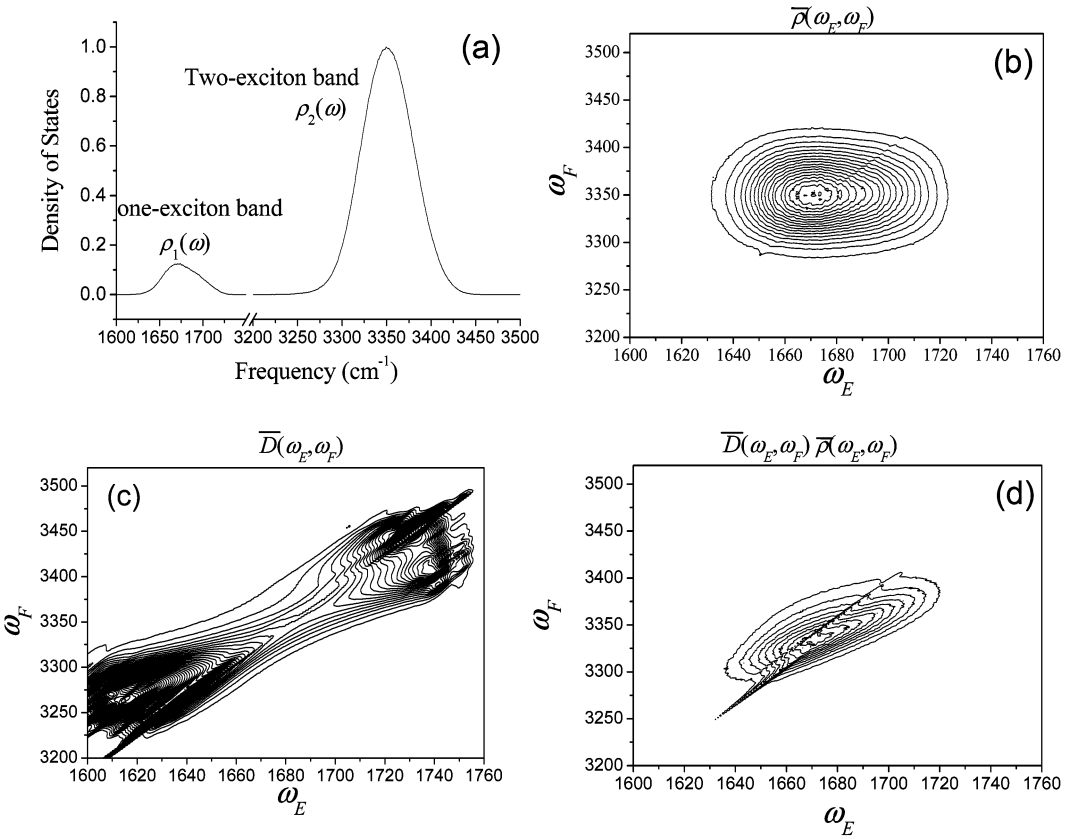

Figure 6. (a) Plot of the density of two-exciton states, $\rho_2(\omega)$, and comparison with $\rho_1(\omega)$. (b) Plot of the ensemble-averaged two-dimensional transition spectral density $\bar{\rho}(\omega_E,\omega_F)$ (see the context for the definition of $\bar{\rho}(\omega_E,\omega_F)$). (c) Plot of the 2D dipole strength spectrum associated with transitions from one-exciton band to two-exciton band, $\bar{D}(\omega_E,\omega_F)$. (d) Plot of the product of $\bar{D}(\omega_E,\omega_F)$ and $\bar{\rho}(\omega_E,\omega_F)$.

the two-dimensional one-quantum absorption spectrum, defined as $\bar{D}(\omega_E,\omega_F)\bar{\rho}(\omega_E,\omega_F)$, and it is plotted in Figure 6d. This 2D spectrum in Figure 6d provides information on the transition probability from one of the one-exciton states, $|e\rangle$ with frequency of ω_E, to one of the two-exciton states, $|f\rangle$ with frequency of ω_F. The 2D line shape of $\bar{D}(\omega_E,\omega_F)\bar{\rho}(\omega_E,\omega_F)$ is largely dictated by the two-dimensional transition density of state, $\bar{\rho}(\omega_E,\omega_F)$, and appears to be diagonally elongated.

B. 2D IR Pump−Probe Nonlinear Response Functions. Now, we will present numerically calculated 2D IR pump−probe spectra of the aqueous PA_{22} solution. Let's consider the six relevant double-sided Feynman diagrams shown in Figure 7. The first two diagrams involve either excited-state population or vibrational coherence evolution $|e_1\rangle\langle e_2|$ during the t_2 period so that these two terms were called stimulated emission (SE) contribution because the probe beam interaction induces an emitting transition down to the ground state. The third and fourth diagrams are combined to contribute to the IR pump−probe signal as the ground-state bleaching (GB) because of the ground-state population evolution during the t_2 period. The transient absorption (TA) contribution is from the sum of the fifth and sixth diagrams. Although in R_1, R_2, R_5, and R_6 diagrams the vibrational coherence states, such as $|e_1\rangle\langle e_2|$ where e_1 and e_2 represent the two different one-exciton states, are involved in the t_2 period, since the width of the one-exciton band is sufficiently broad the pathways with $e_1 \neq e_2$ are destructively interfering with each other so that only the population evolution contribution to R_1, R_2, R_5, and R_6 will survive and significantly contribute to the 2D IR pump−probe signal. Now, by following the same procedure to obtain eq 14 and by assuming that the vibrational dephasing is negligibly small, the ideal 2D IR pump−probe spectrum at time zero, when the polarization

direction of the pump pulse is parallel with that of the probe pulse, can be calculated as

$$S_{\parallel}(\omega_{pu},\omega_{pr}) \propto S_{\parallel}^{SE}(\omega_{pu},\omega_{pr}) + S_{\parallel}^{GB}(\omega_{pu},\omega_{pr}) + S_{\parallel}^{TA}(\omega_{pu},\omega_{pr}) \tag{18}$$

where

$$S_{\parallel}^{SE}(\omega_{pu},\omega_{pr}) = -\frac{1}{15}\langle\sum_{e_1}\sum_{e_2}\{|\mu_{ge1}|^2|\mu_{ge2}|^2(2\cos^2\beta_{e1e2}+1)\}\,\delta(\omega_{pu}-\omega_{e1})\delta(\omega_{pr}-\omega_{e1})\rangle$$

$$S_{\parallel}^{GB}(\omega_{pu},\omega_{pr}) = -\frac{1}{15}\langle\sum_{e_1}\sum_{e_2}\{|\mu_{ge1}|^2|\mu_{ge2}|^2(2\cos^2\beta_{e1e2}+1)\}\,\delta(\omega_{pu}-\omega_{e1})\delta(\omega_{pr}-\omega_{e2})\rangle$$

$$S_{\parallel}^{TA}(\omega_{pu},\omega_{pr}) = +\frac{1}{15}\langle\sum_{e}\sum_{f}\{|\mu_{ge}|^2|\mu_{ef}|^2(2\cos^2\eta_{ef}+1)\}\times\delta(\omega_{pu}-\omega_{e})\delta(\omega_{pr}-\omega_{f}+\omega_{e})\rangle \tag{19}$$

The transition dipole matrix elements were denoted as μ_{ge1}, μ_{ge2}, μ_{ge}, and μ_{ef}. The angle between μ_{ge1} and μ_{ge2} and that between μ_{ge} and μ_{ef} were denoted as β_{e1e2} and η_{ef}, respectively. Now, the corresponding signal when the probe field polarization is perpendicular to the pump field polarization can be immediately written as

$$S_{\perp}(\omega_{pu},\omega_{pr}) \propto S_{\perp}^{SE}(\omega_{pu},\omega_{pr}) + S_{\perp}^{GB}(\omega_{pu},\omega_{pr}) + S_{\perp}^{TA}(\omega_{pu},\omega_{pr}) \tag{20}$$

where

$$S_{\perp}^{SE}(\omega_{pu},\omega_{pr}) = -\frac{1}{15}\langle\sum_{e_1}\sum_{e_2}\{|\mu_{ge1}|^2|\mu_{ge2}|^2(2-\cos^2\beta_{e1e2})\}\times\delta(\omega_{pu}-\omega_{e1})\delta(\omega_{pr}-\omega_{e1})\rangle$$

$$S_{\perp}^{GB}(\omega_{pu},\omega_{pr}) = -\frac{1}{15}\langle\sum_{e_1}\sum_{e_2}\{|\mu_{ge1}|^2|\mu_{ge2}|^2(2-\cos^2\beta_{e1e2})\}\,\delta(\omega_{pu}-\omega_{e1})\delta(\omega_{pr}-\omega_{e2})\rangle$$

$$S_{\perp}^{TA}(\omega_{pu},\omega_{pr}) = +\frac{1}{15}\langle\sum_{e}\sum_{f}\{|\mu_{ge}|^2|\mu_{ef}|^2(2-\cos^2\eta_{ef})\}\times\delta(\omega_{pu}-\omega_{e})\delta(\omega_{pr}-\omega_{f}+\omega_{e})\rangle \tag{21}$$

From eqs 18−21, one can selectively eliminate the diagonal peaks ($e_1 = e_2$) by calculating the following difference spectrum

$$\Delta S(\omega_{pu},\omega_{pr}) = 3S_{\perp}(\omega_{pu},\omega_{pr}) - S_{\parallel}(\omega_{pu},\omega_{pr}) \tag{22}$$

The line broadening induced by the vibrational dephasing process can be approximately taken into account by the following replacements in eqs 19 and 21:

$$\delta(\omega_m-\omega_n) \rightarrow \frac{\Gamma}{(\omega_m-\omega_n)^2+\Gamma^2} \tag{23}$$

In the following numerical calculations, we assume that the vibrational dephasing constant of the coherence state $|e\rangle\langle f|$ is identical to that of $|e\rangle\langle g|$ and it was denoted as Γ (= 8 cm^{-1}) just for numerical calculations.

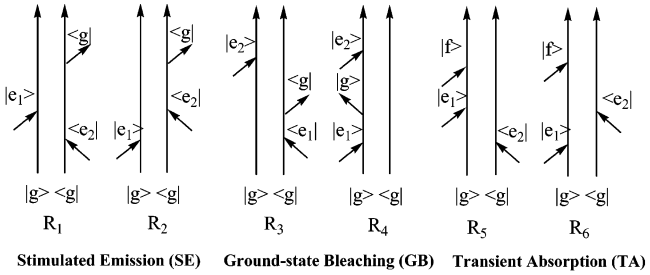

Figure 7. Six double-sided Feynman diagrams associated with the 2D IR pump−probe spectroscopy.

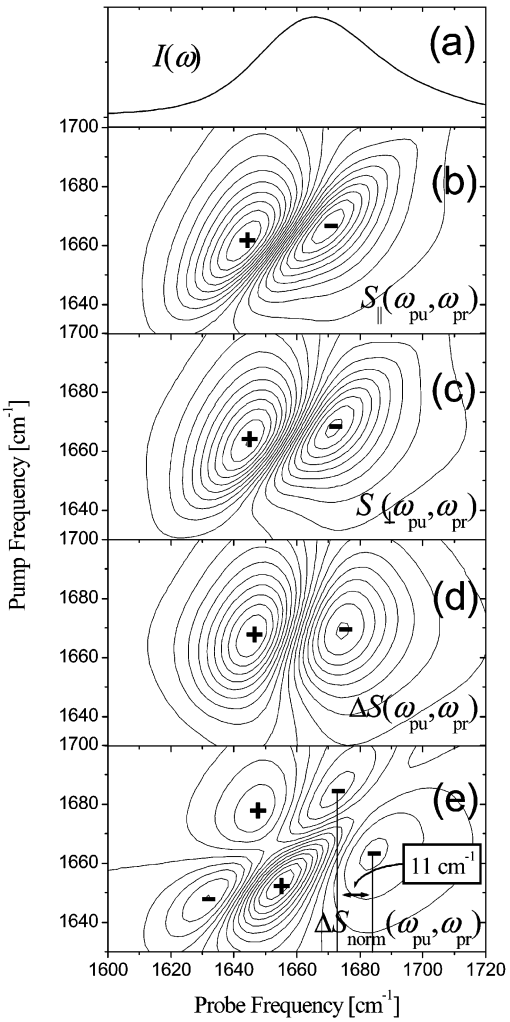

Figure 8. (a) Plot of the amide I IR absorption band in Figure 5b for the sake of comparison: (b) $S_{\parallel}(\omega_{pu},\omega_{pr})$, (c) $S_{\perp}(\omega_{pu},\omega_{pr})$, (d) $\Delta S(\omega_{pu},\omega_{pr})$. (e) Plot of the difference spectrum, $\Delta S_{Norm}(\omega_{pu},\omega_{pr})$, calculated by using eq 24.

C. 2D IR Pump−Probe Spectra. The parallel and perpendicular 2D IR pump−probe spectra calculated by using eqs 18−21 are plotted in parts b and c of Figure 8, respectively. Due to the distributions of one- and two-exciton states, the negative (SE + GB) and positive (TA) peaks exhibit discernible slant features along the diagonal line. Since the two spectra, $S_{\parallel}(\omega_{pu},\omega_{pr})$ and $S_{\perp}(\omega_{pu},\omega_{pr})$, include not only the diagonal peaks but also cross-peaks, the two appear to be similar to each other though the absolute magnitude of $S_{\perp}(\omega_{pu},\omega_{pr})$ is different from that of $S_{\parallel}(\omega_{pu},\omega_{pr})$.

From the theoretical relationship between $S_{\parallel}(\omega_{pu},\omega_{pr})$ and $S_{\perp}(\omega_{pu},\omega_{pr})$, it was believed that the diagonal peaks can be selectively eliminated by calculating the difference spectrum,

$\Delta S(\omega_{pu},\omega_{pr})$, defined in eq 22, and it is plotted in Figure 8d. Surprisingly, the difference spectrum appears to be featureless and broad. This Figure 8d should be compared with Figure 1d in ref 34, where Woutersen and Hamm presented the difference spectrum obtained from experimentally measured $S_{||}(\omega_{pu},\omega_{pr})$ and $S_{\perp}(\omega_{pu},\omega_{pr})$. As reported in ref 34, they clearly observed distinctive cross-peaks, but we do not. At first sight, this notable difference of our numerically calculated $\Delta S(\omega_{pu},\omega_{pr})$ in Figure 8d with theirs appears to be quite puzzling. One may jump into a conclusion that our numerical simulation method in combination with four-site model, eq 1, is not reliable. However, it turns out that their method of obtaining $\Delta S(\omega_{pu},\omega_{pr})$ from $S_{||}(\omega_{pu},\omega_{pr})$ and $S_{\perp}(\omega_{pu},\omega_{pr})$ that were experimentally measured independently is likely to be unreliable to some extent. In practice, the laser pulse intensity varies and fluctuates in time so that the experimentalist cannot quantitatively compare $S_{||}(\omega_{pu},\omega_{pr})$ and $S_{\perp}(\omega_{pu},\omega_{pr})$ directly since these two signals are obtained independently in time. Consequently, they had to normalize the two signals by making the maximum of $|S_{||}(\omega_{pu},\omega_{pr})|$ to be identical to that of $|S_{\perp}(\omega_{pu},\omega_{pr})|$ and obtained $\Delta S_{Norm}(\omega_{pu},\omega_{pr})$ by using the following procedure, i.e.,

$$\Delta S_{Norm}(\omega_{pu},\omega_{pr}) = \frac{S_{\perp}(\omega_{pu},\omega_{pr})}{\max|S_{\perp}(\omega_{pu},\omega_{pr})|} - \frac{S_{||}(\omega_{pu},\omega_{pr})}{\max|S_{||}(\omega_{pu},\omega_{pr})|} \quad (24)$$

where the subscript "Norm" emphasizes that the difference spectrum in this case is obtained by using the normalization procedure. Then, they assumed that the real difference spectrum $\Delta S(\omega_{pu},\omega_{pr})$ is identical to the above difference spectrum $\Delta S_{Norm}(\omega_{pu},\omega_{pr})$. The same method (normalization procedure) was also used to obtain the difference spectra of small oligopeptides such as trialanine in liquid water.[67] In the latter case, where the two amide I normal modes are well defined and the corresponding normal-mode frequencies are well separated, the above assumption (normalization procedure) could be quantitatively reliable—by carrying out MD simulation studies of acetylproline in liquid water and chloroform we have confirmed that this statement is valid and the results will be presented elsewhere. However, we found that the above normalization procedure in eq 24 is not reliable in the case of α-helical PA_{22} solution. To prove this, we also followed the same normalization procedure, calculated the difference spectrum, $\Delta S_{Norm}(\omega_{pu},\omega_{pr})$ using eq 24, and plotted it in Figure 8e. The ratio, $\max|S_{||}(\omega_{pu},\omega_{pr})|/\max|S_{\perp}(\omega_{pu},\omega_{pr})|$, is estimated to be 2.0, and Woutersen and Hamm found that this ratio is close to 2.4—note that in the figure caption of Figure 1 of ref 34 the scales of the contour lines associated with $S_{||}(\omega_{pu},\omega_{pr})$ and $S_{\perp}(\omega_{pu},\omega_{pr})$ were given to be 0.048 mOD(optical density) and 0.020 mOD so that the ratio $\max|S_{||}(\omega_{pu},\omega_{pr})|/\max|S_{\perp}(\omega_{pu},\omega_{pr})|$ estimated from their experiment is about 2.4. Here, it should be emphasized that this ratio strongly deviates from the ideal value of 3. Figure 8e is found to be quantitatively close to the experimental result (compare Figure 8e in the present paper with Figure 1d of ref 34), indicating that our numerically calculated spectra capture most of the salient features and are in good agreement with experiments. Nevertheless, it should be mentioned that Woutersen and Hamm made a conclusive statement that the $A-E_1$ frequency splitting is 10 cm^{-1} since the frequency difference between the two cross-peaks found in Figure 1(d) in ref 34 is about 10 cm^{-1} − note that the same frequency splitting in Figure 8(e) in the present paper is estimated to be about 11 cm^{-1}. However, as discussed above, due to the inequality, $\Delta S \neq \Delta S_{Norm}$, their conclusion regarding to the $A-E_1$ frequency splitting needs to be reexamined in the future. This comparative investigation between the present theoretical studies and experimental results in ref 34 suggests that the normalization procedure of eq 24 for obtaining the difference spectrum should be used carefully particularly when the size of polypeptide is so large that the diagonal peaks are produced by complicated interferences among various contributions from different nonlinear optical transition pathways.

Although we couldn't observe cross-peaks in the difference spectrum of α-helical PA_{22} in liquid water and the validity of previous interpretation of cross-peaks observed in $\Delta S_{Norm}(\omega_{pu},\omega_{pr})$ was questioned, it is believed we have confirmed that our numerical calculation method works well because we were able to reproduce $S_{||}(\omega_{pu},\omega_{pr})$, $S_{\perp}(\omega_{pu},\omega_{pr})$, and $\Delta S_{Norm}(\omega_{pu},\omega_{pr})$ that were experimentally measured.

VI. Summary and a Few Concluding Remarks

Amide I vibrational dynamics of α-helical polyalanines has been studied in the present paper. Carrying out extensive AM1 calculations of various α-helical polyalanines with varying chain length, we found (1) that the vibrational coupling constants are not dependent on the chain length and (2) that the amide I local mode frequency depends on the location of the peptide bond in a given α-helix. We showed that the corresponding Hessian matrix in the amide I local mode subspace can be theoretically constructed by using the extrapolation method developed recently by the authors. To understand the hydrogen-bonding dynamics between α-helical polyalanine having 22 peptide bonds and surrounding water molecules, classical MD simulation study was performed. The conformational fluctuation amplitude and amide I local mode frequency correlation functions were calculated. It turns out that the correlation times of amide I local mode frequency fluctuations are so slow that the line broadening is largely determined by the inhomogeneous distribution of the instantaneous conformations. Therefore, the instantaneous normal mode (INM) analysis method was used to obtain densities of states of both one- and two-exciton bands. To study the nature of amide I INMs in terms of either *A*-mode-like or E_1-mode-like behavior, we introduced a novel function, i.e., weighted phase-correlation factor (WPCF), which can vary from $-1 + {}^1/_N$ to $1 - {}^1/_N$ with N being the number of peptide bonds. On the basis of the ensemble-averaged WPCF spectra, we found that there is no unique way to classify a given amide I INM to be either *A*- or E_1-mode-like.

Using the MD simulation and INM analysis results, we calculated the amide I IR absorption spectrum and compared it with experiment. Although the center frequency of numerically calculated IR absorption spectrum is about 40 cm^{-1} higher than that of the experimental one, the asymmetric line shape is in excellent agreement with the experiment. However, the more stringent test on the validity of our numerical calculation methods was to make direct comparisons of the numerically calculated 2D IR pump−probe spectra with those experimentally measured by Woutersen and Hamm. The 2D line shapes of both the parallel and perpendicular IR pump−probe spectra, i.e., $S_{||}(\omega_{pu},\omega_{pr})$ and $S_{\perp}(\omega_{pu},\omega_{pr})$, respectively, were found to be in good agreement with theirs. However, the ideal difference spectrum, which was defined as $3S_{\perp}(\omega_{pu},\omega_{pr}) - S_{||}(\omega_{pu},\omega_{pr})$, was found to be featureless and broad, though Woutersen and Hamm's difference spectrum clearly exhibited cross-peaks revealing the $A-E_1$ frequency splitting to be 10 cm^{-1}. It turned out that this notable difference between the difference spectrum in the present paper and theirs originates from the difference in obtaining difference spectrum. They used normalization method to obtain the difference spectrum instead of directly calculating

$3S_{\perp}(\omega_{pu},\omega_{pr}) - S_{\parallel}(\omega_{pu},\omega_{pr})$ from the two spectra, $S_{\parallel}(\omega_{pu},\omega_{pr})$ and $S_{\perp}(\omega_{pu},\omega_{pr})$. Following the same normalization method to obtain the difference spectrum, we showed that our $\Delta S_{Norm}(\omega_{pu},\omega_{pr})$ is in good agreement with their difference spectrum. This observation suggests that, unlike small polypeptides such as tri-alanine, the normalization method to obtain the difference spectrum should be used carefully as long as the chain-length of the polypeptide is so long that the one- and two-quantum excited states form bands instead of well-defined and frequency-resolved quantum states.

Although we presented 2D IR pump−probe spectra of an aqueous α-helical polyalanine solution, we could not predict the time-evolution of the 2D spectra. This is because the current theory is not capable of taking into account the dynamical correlations of different INMs nor vibrational energy redistributions within the one- and two-exciton bands. We are currently developing a theoretical method by considering energy diffusion equation and by numerically calculating time-dependent spectra.

Acknowledgment. This work was supported by the Creative Research Initiatives Program of KISTEP (MOST, Korea).

References and Notes

(1) Surewicz, W. K.; Mantsch, H. H. In *Spectroscopic Methods for Determining Protein Structure in Solution*; Havel, H. A., Ed.; VCH: New York, 1996; p 135.
(2) Gremlich, H.-U.; Yan, B. *Infrared and Raman Spectroscopy of Biological Materials*; Marcel Dekker: New York, 2000.
(3) Krimm, S.; Bandekar, J. *Adv. Protein Chem.* **1986**, *38*, 181.
(4) Krimm, S.; Abe, Y. *Proc. Natl. Acad. Sci. U.S.A.* **1972**, *69*, 2788. Moore, W. H.; Krimm, S. *Proc. Natl. Acad. Sci. U.S.A.* **1975**, *72*, 4933.
(5) Moore, W. H.; Krimm, S. *Biopolymers* **1976**, *15*, 2465.
(6) Dwivedi, A. M.; Krimm, S. *Macromolecules* **1982**, *15*, 186; **1983**, *16*, 340.
(7) Torii, H.; Tasumi, M. *J. Chem. Phys.* **1992**, *96*, 3379.
(8) Torii, H.; Tasumi, M. In *Infrared Spectroscopy of Biomolecules*; Wiley-Liss: New York, 1996; p 1.
(9) Ramek, M.; Yu, C.-H.; Schafer, L. *Can. J. Chem.* **1998**, *76*, 566.
(10) Kubelka, J.; Keiderling, T. A. *J. Phys. Chem. A* **2001**, *105*, 10922; *J. Am. Chem. Soc.* **2001**, *123*, 6142; **2001**, *123*, 12048.
(11) Bour, P.; Kubelka, J.; Keiderling, T. A. *Biopolymers* **2000**, *53*, 380.
(12) Silva, R. A. G. D.; Kubelka, J.; Bour, P.; Decatur, S. M.; Keiderling, T. A. *Proc. Natl. Acad. Sci. U.S.A.* **2000**, *97*, 8318.
(13) Mirkin, N. G.; Krimm, S. *J. Phys. Chem. A* **2002**, *106*, 3391.
(14) Mu, Y.; Stock, G. *J. Phys. Chem.* B **2002**, *106*, 5294.
(15) Hamm, P.; Lim, M.; Hochstrasser, R. M. *J. Phys. Chem. B* **1998**, *102*, 6123.
(16) Scheurer, C.; Piryatinski, A.; Mukamel, S. *J. Am. Chem. Soc.* **2001**, *123*, 3114.
(17) Ham, S.; Kim, J.-H.; Lee, H.; Cho, M. *J. Chem. Phys.* **2003**, *118*, 3491.
(18) Kwac, K.; Cho, M.; *J. Chem. Phys.* **2003**, *119*, 2247.
(19) Brauner, J. W.; Dugan, C.; Mendelsohn, R. *J. Am. Chem. Soc.* **2000**, *122*, 677.
(20) Arrondo, J. L. R.; Goni, F. M. *Prog. Biophys. Mol. Biol.* **1999**, *72*, 367.
(21) Byler, D. M.; Susi, H. *Biopolymer* **1986**, *25*, 469.
(22) Surewicz, W. K.; Mantsch, H. H. *Biochim. Biophys. Acta* **1988**, *952*, 115.
(23) Jackson, M.; Haris, P. I.; Chapman, D. *J. Mol. Struct.* **1989**, *214*, 329.
(24) Mantsch, H. H.; Casal, H. L.; Jones, R. N. In *Spectroscopy of Biological Systems, Advances in Spectroscopy*; Clark R. J. H., Hester, R. E., Eds.; Wiley: New York, 1986; Vol. 13, p 1.
(25) Mantsch, H. H.; Surewics, W. K.; Chapman, D. *Biochemistry* **1993**, *32*, 389.
(26) Chen, X. G.; Asher, S. A.; Schweitzer-Stenner, R.; Mirkin, N. G.; Krimm, S. *J. Am. Chem. Soc.* **1995**, *117*, 2884. Chi, Z.; Chen, X. G.; Holtz, J. S. W.; Asher, S. A. *Biochemistry* **1998**, *37*, 2854.
(27) Schweitzer-Stenner, R. *J. Raman Spectrosc.* **2001**, *32*, 711.
(28) Berova, N.; Nakanishi, K.; Woody, R. W. *Circular Dichroism, Principles and Applications*; Wiley-VCH: New York, 2000.
(29) Barron, L. D.; Hecht, L.; Bell, A. F.; Wilson, G. *Appl. Spectrosc.* **1996**, *50*, 619.
(30) Hamm, P.; Lim, M.; Hochstrasser, R. M. *J. Phys. Chem. B* **1998**, *102*, 6123.
(31) Hamm, P.; Lim, M.; DeGrado, W. F.; Hochstrasser, R. M. *Proc. Natl. Acad. Sci. U.S.A.* **1999**, *96*, 2036.
(32) Moran, A. M.; Park, S.-M.; Dreyer, J.; Mukamel, S. *J. Chem. Phys.* **2003**, *118*, 3651.
(33) Cho, M. In *Advances in Multi-Photon Processes and Spectroscopy*; Lin, S. H., Villaeys, A. A., Fujimura Y., Eds.; World Scientific: Singapore, 1999; Vol. 12, p 229.
(34) Woutersen, S.; Hamm, P. *J. Chem. Phys.* **2001**, *115*, 7737.
(35) Zanni, M. T.; Gnanakaran, S.; Stenger, J.; Hochstrasser, R. M. *J. Phys. Chem. B* **2001**, *105*, 6520.
(36) Cho, M. *PhysChemComm* **2002**, *5*, 40.
(37) Woutersen, S.; Pfister, R.; Hamm, P.; Mu, Y.; Kosov, D. S.; Stock, G. *J. Chem. Phys.* **2002**, *117*, 6833.
(38) Choi, J.-H.; Ham, S.; Cho, M. *J. Chem. Phys.* **2003**, *117*, 6821.
(39) Cha, S.; Ham, S.; Cho, M. *J. Chem. Phys.* **2003**, *117*, 740.
(40) Cho, M. *J. Chem. Phys.* **2003**, *118*, 3480.
(41) Ham, S.; Cho, M. *J. Chem. Phys.* **2003**, *118*, 6915.
(42) Ham, S.; Cha, S.; Choi, J.-H.; Cho, M. *J. Chem. Phys.* **2003**, *119*, 1451.
(43) Choi, J.-H.; Ham, S.; Cho, M. *J. Phys. Chem. B* **2003**, *107*, 9132.
(44) Kwac, K.; Cho, M. *J. Chem. Phys.* **2003**, *119*, 2256.
(45) Kwac, K.; Lee, H.; Cho, M. *J. Chem. Phys.* **2004**, *120*, 1477.
(46) Dewar, M.; Thiel, W. *J. Am. Chem. Soc.* **1977**, *99*, 4499; Dewar, M.; Zoebisch, E. G.; Healy, E. F. *J. Am. Chem. Soc.* **1985**, *107*, 3902.
(47) Lednev, I. K.; Karnoup, A. S.; Sparrow, M. C.; Asher, S. A. *J. Am. Chem. Soc.* **1999**, *121*, 4076; **1999**, *121*, 8074; **2001**, *123*, 2388.
(48) Ianoul, A.; Mikhonin, A.; Lednev, I. K.; Asher, S. A. *J. Phys. Chem. A.* **2002**, ***106***, 3621.
(49) Lockhart, D. J.; Kim, P. S. *Sicence* **1992**, *257*, 947; **1993**, *260*, 198.
(50) Thompson, P. A.; Eaton, W. A.; Hofrichter, J. *Biochemistry* **1997**, *36*, 6, 9200.
(51) Dyer, R. B.; Gai, F.; Woodruff, W. H. *Acc. Chem. Res.* **1998**, *31*, 709.
(52) Thompson, P. A.; Munoz, V.; Jas, G. S.; Henry, E. R.; Eaton, W. A.; Hofrichter, J. *J. Phys. Chem. B* **2000**, *104* 378.
(53) Garcia, A. E.; Sanbonmatsu, K. Y. *Proc. Natl. Acad. Sci. U.S.A.* **2002**, *99*, 2782.
(54) Case, D. A.; Pearlman, D. A.; Caldwell, J. W. et al. *AMBER 7*; University of California: San Francisco, 2002.
(55) Darden, T.; York, D.; Pedersen, L. *J. Chem. Phys.* **1993**, *98*, 10089.
(56) Berendsen, H. J. C.; Postma, J. P. M.; van Gunsteren, W. F.; DiNola, A.; Haak, J. R. *J. Chem. Phys.* **1984**, *81*, 3684.
(57) Fersht, A. In *Structure and Mechanism in Protein Science*; W. H. Freeman and Co.: New York, 2000; p 17.
(58) Decatur, S. M.; Antonic, J. *J. Am. Chem. Soc.* **1999**, *121*, 11914
(59) Silva, P. A. G. D.; Nguyen, J. Y.; Decatur, S. M. *Biochemistry* **2002**, *41*, 15296.
(60) Liu, H.; Elstner, M.; Kaxiras, E.; Frauenheim, T.; Hermans, J.; Yang, W. *Proteins: Struct., Funct., Genet.* **2001**, *44*, 484.
(61) Cho, M.; Fleming, G. R.; Saito, S.; Ohmine, I.; Stratt, R. M. *J. Chem. Phys.* **1994**, *100*, 6672.
(62) Stratt, R. M.; Maroncelli, M. *J. Phys. Chem.* **1996**, *100*, 12981.
(63) Ladanyi, B. M.; Stratt, R. M. *J. Phys. Chem.* **1996**, *100*, 1266.
(64) Keyes, T. *J. Phys. Chem. A* **1997**, *101*, 2921.
(65) Krimm, S.; Reisdorf, W. C., Jr. *Faraday Discuss* **1994**, *99*, 181.
(66) Torii, H.; Tasumi, M. *J. Chem. Phys.* **1992**, *97*, 86.
(67) Woutersen, S.; Hamm, P. *J. Chem. Phys.* **2001**, *114*, 2727.